IL NUOVO CIMENTO Vol. 36 C, N. 6 Novembre-Dicembre 2013
DOI 10.1393/ncc/i2014-11651-4

Colloquia: LaThuile13

Higgs boson studies at CMS

N. Chanon for the CMS Collaboration
Eidgenoessische Tech. Hochschule - Zürich, Switzerland

ricevuto il 20 Giugno 2013; approvato l'1 Luglio 2013

Summary. — Higgs boson studies at the Compact Muon Solenoid (CMS) with an integrated luminosity of $5\,\text{fb}^{-1}$ at 7 TeV and up to $12.2\,\text{fb}^{-1}$ at 8 TeV in the center of mass are presented. After a brief description of the CMS detector and production and decay of the Higgs boson at the LHC, the main Higgs analyses at CMS are described: $H \to \gamma\gamma$, $H \to ZZ$, $H \to W^+W^-$, $H \to b\bar{b}$, $H \to \tau^+\tau^-$. The statistical combination of the results from all channels is presented. The new particle existence is now well established, with an observed significance of 6.9σ, a signal strength $\mu = 0.88 \pm 0.21$ times the standard model and a measured mass $m_H = 125.8 \pm 0.4(\text{stat.}) \pm 0.4(\text{syst.})$ GeV. No significant deviation from the standard model Higgs boson hypothesis was found.

PACS 14.80.Bn – Standard model Higgs boson.

1. – Introduction

In the standard model of particle physics, vector boson masses arise from the spontaneous breaking of electroweak symmetry by the Higgs field while the fermion masses are generated via the Yukawa couplings. A new boson was discovered in July 2012 in the Higgs boson searches [1, 2], with a mass around 125 GeV, so far compatible with the standard model Higgs boson hypothesis. In these proceedings, we will first introduce the CMS detector and Higgs boson production and decay at the LHC, then focus on updates of Higgs boson searches at CMS in the decay channels $H \to \gamma\gamma$, $H \to ZZ$, $H \to W^+W^-$, $H \to b\bar{b}$, $H \to \tau^+\tau^-$. The statistical combination of the results from all channels will also presented.

2. – CMS detector

A detailed description of the CMS detector can be found in [3]. The key components of the detector include a silicon pixel and a silicon strip tracker, embedded in a 3.8 T solenoidal magnetic field, used to measure the momentum of charged particles. The silicon pixel and strip tracking system covers the pseudorapidity range $|\eta| < 2.5$, where

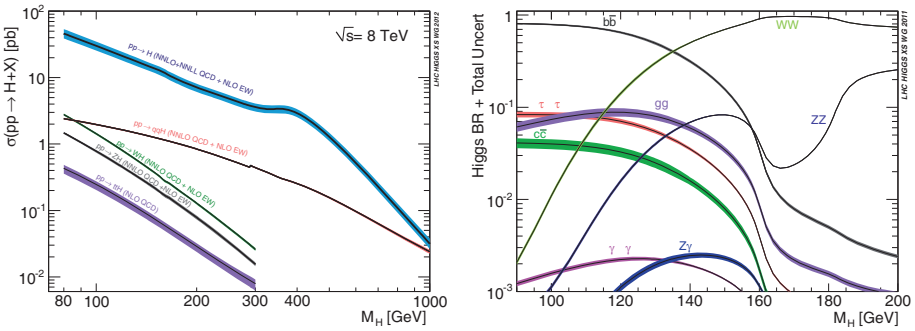

Fig. 1. – Higgs production cross-sections (left) and branching ratio (right) [4].

$\eta = -\ln[\tan(\theta/2)]$, and θ is the polar angle of the trajectory of the particle with respect to the beam direction. It is surrounded by a lead tungstate crystal electromagnetic calorimeter (ECAL) and a brass-scintillator hadron calorimeter (HCAL). The ECAL and HCAL extend to a pseudorapidity range of $|\eta| < 3.0$. A steel/quartz-fiber Cherenkov forward detector (HF) extends the calorimetric coverage to $|\eta| < 5.2$. The calorimeters are surrounded by the muon system, used to identify muons and measure their momentum. The muon system consists of gas detectors placed in the steel return yoke of the magnet. The high instantaneous luminosity delivered by the LHC provides an average of about 9 (21) pile-up interactions per bunch crossing in 2011 (2012). Analysis presented in this proceeding are using an integrated luminosity of $5\,\text{fb}^{-1}$ at 7 TeV acquired in 2011 and up to $12.2\,\text{fb}^{-1}$ at 8 TeV in the center of mass acquired in 2012.

3. – Higgs boson production and decay

At the LHC, due to high gluon luminosity inside the proton, the Higgs boson is mainly produced via gluon fusion, followed by vector boson fusion (VBF) with an order of magnitude lower rate, associated production with a vector boson and $t\bar{t}$ fusion, as shown in fig. 1. As it is essential to probe Higgs coupling to bosons and fermions, the main decay channels where the search is performed are $H \to \gamma\gamma$, $H \to ZZ$, $H \to W^+W^-$, $H \to b\bar{b}$, $H \to \tau^+\tau^-$. Analyses presented are listed in table I.

TABLE I. – *Higgs boson decay channels presented with their accessible mass range, resolution and integrated luminosity* $(7 + 8\,\text{TeV})$ *analyzed.*

Decay channel	Mass range (GeV)	Mass resolution	Luminosity (fb^{-1})
$H \to b\bar{b}$	110–135	10%	$5.0 + 12.2$
$H \to \tau^+\tau^-$	110–140	20%	$5.0 + 12.1$
$H \to W^+W^- \to 2l2\nu$	110–1000	20%	$4.9 + 12.1$
$H \to ZZ \to 4l$	110–1000	1–2%	$5.1 + 12.2$
$H \to \gamma\gamma$	110–150	1–2%	$5.1 + 5.3$

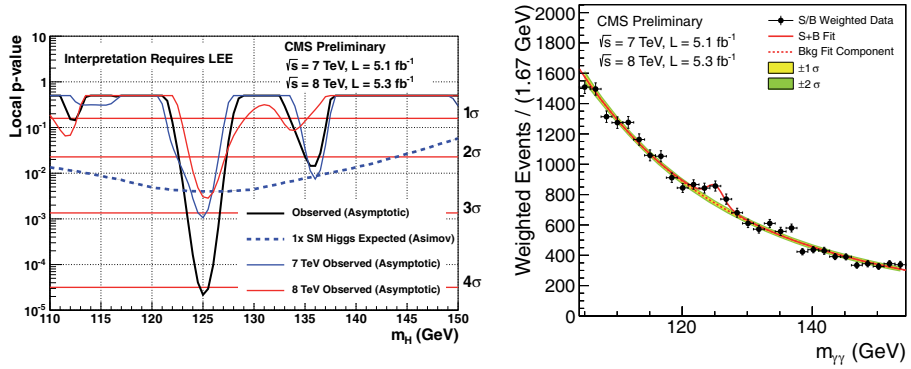

Fig. 2. – Local p-value observed in the $H \to \gamma\gamma$ channel with the main analysis (left) and weighted $\gamma\gamma$ mass spectrum in data.

4. – Higgs searches in the $H \to \gamma\gamma$ channel

The $H \to \gamma\gamma$ analysis [5] has an excellent mass resolution (1–2%) and sensibility for a low mass Higgs. Main backgrounds are QCD production of dijet, $\gamma +$ jets, and diphotons, the later being irreducible. The $H \to \gamma\gamma$ signature consists in two high p_T isolated photons arising from the same vertex. The main analysis uses multivariate techniques to select and classify events, while another analysis with sequential selection is used as cross-check. Correctly determining the opening angle between the photons is an important ingredient for improving the mass resolution, thus a boosted decision tree (BDT) is used for finding the primary vertex of the events among all pile-up vertices. Photon identification is performed with a BDT using shower shape and isolation variables to reduce the background arising from jets. Energy regression with a BDT is used to improve the $\gamma\gamma$ mass resolution and its performance is controled with $Z \to ee$ events. The output of those BDTs is feed to a Diphoton BDT using kinematics, vertexing, photon identification and energy resolution, used to categorize the events. Four diphoton "untagged" categories are defined in the Diphoton BDT output. Two "VBF-tag" categories are also defined aiming at selecting primarily VBF events. Analysis sensitivity is estimated from a fit to the diphoton invariant mass spectrum in each categories. Bernstein polynomials of various order are selected for the background modeling, and the order is chosen by selecting the lowest one preserving a bias smaller than 20% of the statistical uncertainty. The observed local significance is above 4.1σ (see fig. 3) and the measured best fit value is found to be $\mu = 1.45 \pm 0.53$ times the standard model cross-section for a Higgs boson mass of 125 GeV. The diphoton mass spectrum observed in data merging all categories and weighting their contribution by signal over background (s/b) in each categories is shown in fig. 2 and shows clearly the presence of a signal.

5. – Higgs searches in the $H \to ZZ$ channel

The $H \to ZZ \to 4l$ channel [6] is very interesting for searching a Higgs boson at low mass because of its excellent mass resolution (1–2%) and good s/b ratio ($s/b \backsimeq 2$). Main background is the irreducible ZZ, followed by $Z +$ jets and $t\bar{t}$. Event topology searched for is four isolated lepton final state emerging from the same vertex. In order not to loose signficant signal efficiency, one needs to select lepton transverse momentum

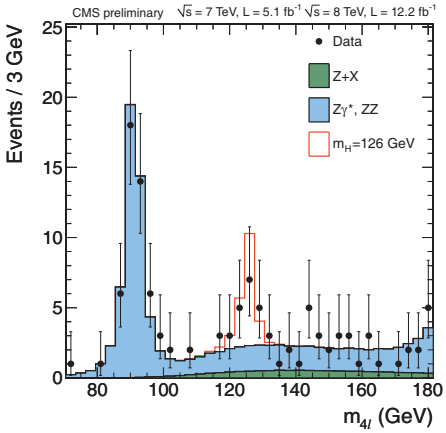

Fig. 3. – Invariant mass spectrum in the $H \to ZZ$ channel.

as low as $p_T > 7\,\text{GeV}$ (electrons) and $p_T > 5\,\text{GeV}$ (muons) on the fourth lepton. Four signatures are investigated: 4μ, $2e2\mu$, $4e$ and $2l2\tau$ (high mass only). The invariant mass in the 4μ, $2e2\mu$, $4e$ at 7 and 8 TeV combined is presented in fig. 3 and shows clearly the presence of a signal around 126 GeV. The contribution near 91 GeV is due to the $Z \to 4l$ process and used as a control sample. The number of events observed in data is in agreement with signal and background expectations. A kinematic discriminant (KD) [7] using the angular information of $H \to ZZ \to 4l$ decay as well as the mass of the first and second Z^0 is used to improve the background discrimination. An excess of events compatible with a Higgs boson signal is also found at high values of the KD. A three dimension fit is performed to estimate the analysis sensitivity, using the ZZ invariant mass, uncertainty on the invariant mass and the KD. The observed significance is observed to be 5σ, leading to a discovery in the $H \to ZZ$ channel alone. The best fit value is $\mu = 0.80^{+0.35}_{-0.28}$ at 126 GeV and the mass of the excess is measured to be $m_H = 126.2 \pm 0.6(\text{stat.}) \pm 0.2(\text{syst.})$ (see fig. 4).

6. – Higgs searches in the $H \to W^+W^-$ channel

Strength of $H \to W^+W^-$ decay channel [8] is the relatively large branching ratio, balanced by its relatively low mass resolution (about 20%) due to missing energy in the final state. The analysis signature looked for is two isolated leptons with $p_T > 20, 10\,\text{GeV}$ and missing transverse energy arising for neutrinos escaping detection. Main background to $H \to W^+W^-$ analysis are the irreducible WW, top and W + jets, and are estimated from control regions in data. To improve backgground discrimination, a categorization is performed according to the presence of zero, one or two jets in the events. Lepton final states considered are ee, $e\mu$ and $\mu\mu$, the channel $e\mu$ being the most sensitive due to lower Drell-Yan contribution. Analysis sensitivity is estimated with cut and count method for all channels but the zero and one jet bin in the $e\mu$ lepton flavour, where a shape analysis with a fit in the two dimension of transverse mass and dilepton mass is used. A broad excess is observed in exclusion limits, which is compatible with the presence of a signal. The best fit signal strength is found to be $\mu = 0.74 \pm 0.25$ at 125 GeV. The observed local significance expected is 4.1σ and measured is 3.1σ, as can be seen from fig. 5.

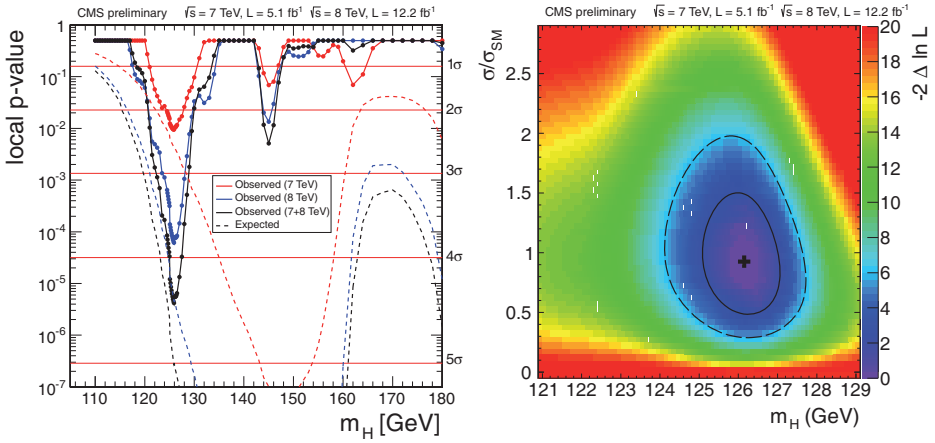

Fig. 4. – Local p-value observed in the $H \to ZZ$ channel (left) and the ratio of measured cross-section over standard model cross-section as a function of the Higgs boson mass hypothesis (right).

7. – Higgs searches in the $H \to b\bar{b}$ channel

The $H \to b\bar{b}$ [9] channel is particularly important to probe Higgs coupling to fermions. Because of the overwhelming background of QCD multijets, the search in the $H \to b\bar{b}$ channel is performed in the associated production mode with a vector boson, which gives additional handle for background rejection. Five channels are considered depending on the decay of the vector boson: $W \to e\nu$, $W \to \mu\nu$, $Z \to ee$, $Z \to \mu\mu$, $Z \to \nu\nu$. Events are triggered accordingly, requiring either one or two leptons or missing transverse energy. To improve the signal to background discrimination, events are further categorized with the vector boson p_T (below and higher than 170 GeV but for $Z \to ll$ where 100 GeV was found to be optimal). The $H \to b\bar{b}$ decay is reconstructed selecting two central b-tagged [10] jets. A b-jet energy regression is trained to improve the reconstructed mass resolution,

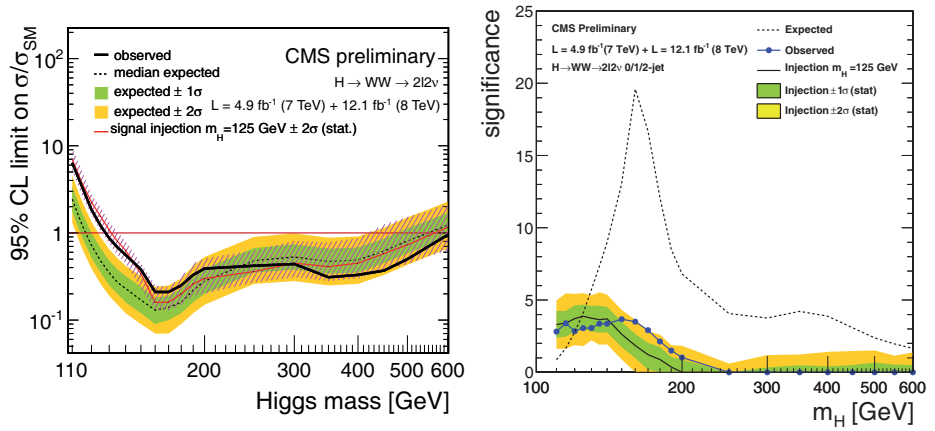

Fig. 5. – Exclusion limits (left) and local p-value observed in the $H \to WW$ channel (right).

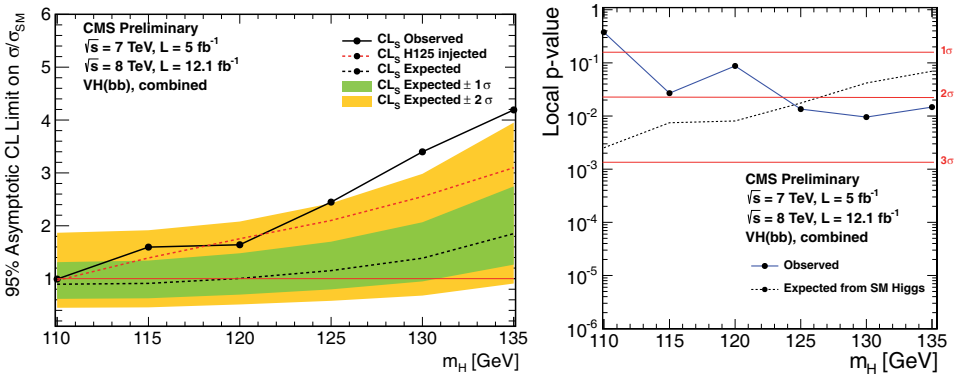

Fig. 6. – Exclusion limits (left) and local p-value observed in the $H \to b\bar{b}$ channel (right).

using secondary vertex and jet properties, missing transverse energy direction and soft lepton information inside the jet, which makes better the overall analysis sensitivity by 15 to 20%. The dijet mass resolution is close to 10%. In each of the channels, a boosted decision tree is used to increase the discrimination against background (mainly vector boson plus jets, dibosons and top), which takes as input jets and vector bosons kinematics and b-tagging discriminant information. A shape analysis of the BDT output is performed in each channel which leads to an improvement of 10% with respect to the case where only a sequential criterion on the BDT output is used. A broad excess is observed in the whole mass range where the analysis is performed, compatible with injection of signal. At 125 GeV, an observed significance of 2.2σ is measured as well as a best fit signal strength $\mu = 1.3^{+0.7}_{-0.6}$ (see fig. 6).

8. – Higgs searches in the $H \to \tau^+\tau^-$ channel

$H \to \tau^+\tau^-$ [11] is another accessible channel allowing to probe the Higgs coupling to fermions. The search is performed in five final states depending on if the τ lepton

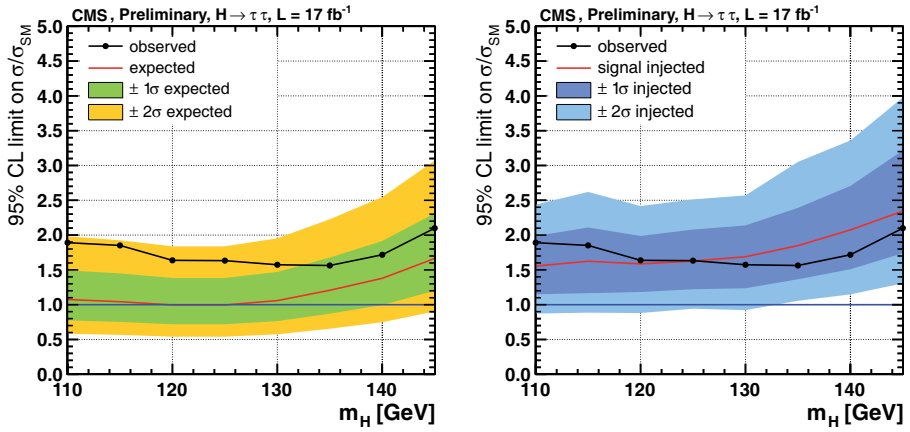

Fig. 7. – Exclusion limits (left) with signal injected (right) in the $H \to \tau^+\tau^-$ channel (right).

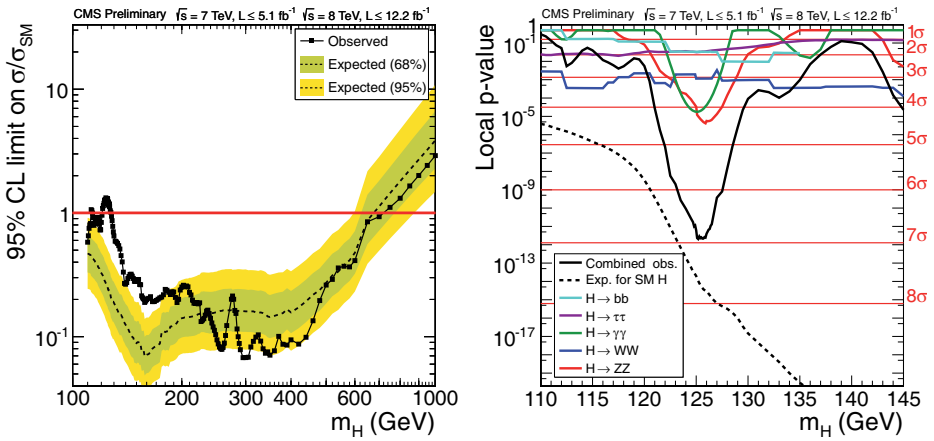

Fig. 8. – Combined exclusion limits at 95% CL for a standard model Higgs boson (left) zoomed in the low mass region (right).

decays into electron (e), muon (μ) or hadronically (τ_h): $\mu\tau_h$, $e\tau_h$, $e\mu$, $\tau_h\tau_h$, $\mu\mu$. Main backgrounds are arising from QCD dijets and $Z \to \tau\tau + \text{jets}$. τ leptons are reconstructed with the Particle-Flow algorithm [12]. τ are required to be isolated, using a multi-variate analysis with isolation rings around the τ. The missing transverse energy definition is improved with a multi-variate technique to decrease the dependence of its resolution with the pile-up. The $\tau\tau$ invariant mass is reconstructed with a matrix element method to improve the mass resolution, instead of considering only the visible $\tau\tau$ mass. Events are categorized according to the presence of zero (not used for sensitivity), one or two jets in the event ("VBF-tag" which has the highest sensitivity). Data-driven methods are used to estimate the τ fake rate from control regions. A broad excess is observed in the exclusion limits, compatible with the signal injection test (see fig. 7), and the best fit signal strength is measured as $\mu = 0.7 \pm 0.5$.

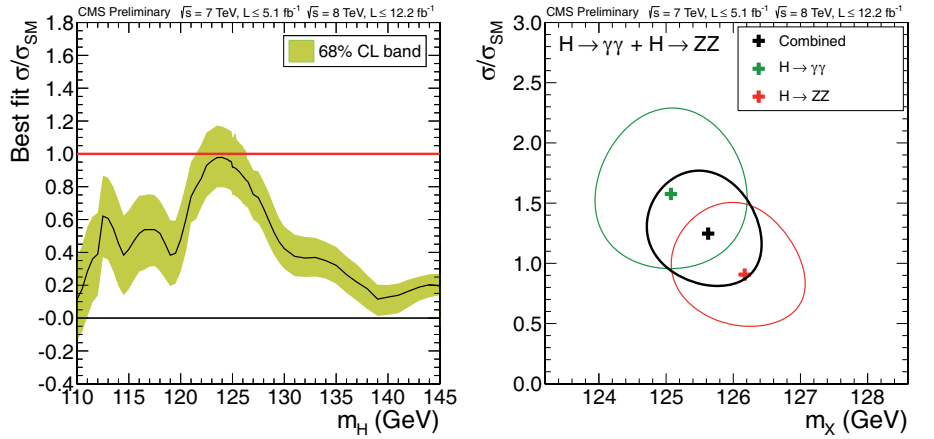

Fig. 9. – Combined local p-value (left) and best fit signal strength (right) for a standard model Higgs boson.

9. – Channel combination

In addition to the channels presented in the previous sections, the CMS Higgs combination takes also as input the results of the following analyses: $WH(\to WW)$, $H \to ZZ \to 2l2\nu$ at high mass, $t\bar{t}H(\to b\bar{b})$ probing the Higgs coupling to top quark, the three of them with $4.9\,\text{fb}^{-1}$ at 7 TeV and $5.1\,\text{fb}^{-1}$ at 8 TeV, and $H \to WW \to l\nu jj$ at high mass with $4.9\,\text{fb}^{-1}$ at 7 TeV and $12.2\,\text{fb}^{-1}$ at 8 TeV, which will not be described here. Exclusion limits at 95% confidence level for the combined results are shown on fig. 8. The whole mass range between 110 GeV and 700 GeV is excluded at 95% CL, but a narrow range [120–127] GeV where an excess is observed. The combined local observed significance of the excess is 6.9σ (while the expected was 7.8σ). As shown on fig. 9, the best fit signal strength is $\mu = 0.88 \pm 0.21$. The mass of the excess is measured using the $H \to \gamma\gamma$ and $H \to ZZ$ channels only since they have the best mass resolution: $m_H = 125.8 \pm 0.4(\text{stat.}) \pm 0.4(\text{syst.})\,\text{GeV}$. Masses measured from $H \to \gamma\gamma$ and $H \to ZZ$ alone are compatible within 1σ.

10. – Conclusions

Results of searches for the standard model Higgs boson at CMS were presented using up to $5\,\text{fb}^{-1}$ at 7 TeV and up to $12.2\,\text{fb}^{-1}$ at 8 TeV in the channels $H \to \gamma\gamma$, $H \to ZZ$, $H \to W^+W^-$, $H \to b\bar{b}$, $H \to \tau^+\tau^-$. An excess is observed at a mass $m_H = 125.8 \pm 0.4(\text{stat.}) \pm 0.4(\text{syst.})\,\text{GeV}$ with a significance of 6.9σ. The best fit signal strength is 0.88 ± 0.21 times the standard model cross-section. There are indication of coupling of the new boson to fermions through $H \to \tau^+\tau^-$ and $H \to b\bar{b}$ channels even if no evidence has been found yet. No significant deviation from the standard model Higgs boson hypothesis was found.

REFERENCES

[1] CMS Collaboration, *Phys. Lett. B*, **716** (2012) 30.
[2] ATLAS Collaboration, *Phys. Lett. B*, **716** (2012) 1-29.
[3] CMS Collaboration, *JINST*, **3** (2008) S08004.
[4] LHC Higgs Cross Section Working Group, arXiv:1201.3084 [hep-ph].
[5] CMS Collaboration, CMS-PAS-HIG-12-015 (2012).
[6] CMS Collaboration, CMS-PAS-HIG-12-041 (2012).
[7] Gao Y. *et al.*, *Phys. Rev. D*, **81** (2010) 075022.
[8] CMS Collaboration, CMS-PAS-HIG-12-042 (2012).
[9] CMS Collaboration, CMS-PAS-HIG-12-044 (2012).
[10] CMS Collaboration, CMS-PAS-BTV-11-003 (2011).
[11] CMS Collaboration, CMS-PAS-HIG-12-043 (2012).
[12] CMS Collaboration, CMS-PAS-PFT-09-001 (2009).